

Energy relaxations of hot electrons in AlGaN/AlN/GaN heterostructures grown by MOCVD on sapphire and 6H-SiC substrates

A. Ilgaz¹, S. Gökden^{1,a}, R. Tülek¹, A. Teke¹, S. Özçelik², and E. Özbay³

¹ Department of Physics, Faculty of Science and Letter, Balıkesir University, Çağış Kampüsü, 10145 Balıkesir, Turkey

² Department of Physics, Faculty of Science and Letter, Gazi University, Teknikokullar, 06500 Ankara, Turkey

³ Department of Physics, Department of Electrical and Electronics Engineering, Nanotechnology Research Center-NANOTAM, Bilkent University, 06800 Ankara, Turkey

Received: 4 May 2011 / Accepted: 23 May 2011

Published online: 18 August 2011 – © EDP Sciences 2011

Abstract. In this work, we investigated the hot-electron dynamics of AlGaN/GaN HEMT structures grown by MOCVD on sapphire and SiC substrates at 80 K. High-speed current-voltage measurements and Hall measurements over the temperature range 27–300 K were used to study hot-electron dynamics. At low fields, drift velocity increases linearly, but deviates from the linearity toward high electric fields. Drift velocities are deduced as approximately 6.55×10^6 and 6.60×10^6 cm/s at an electric field of around $E \sim 25$ kV/cm for samples grown on sapphire and SiC, respectively. To obtain the electron temperature as a function of the applied electric field and power loss as a function of the electron temperature, we used the so-called mobility comparison method with power balance equations. Although their low field carrier transport properties are similar as observed from Hall measurements, hot carrier energy dissipation differs for samples grown on sapphire and SiC substrates. We found that LO-phonon lifetimes are 0.50 ps and 0.32 ps for sapphire and SiC substrates, respectively. A long hot-phonon lifetime results in large non-equilibrium hot phonons. Non-equilibrium hot phonons slow energy relaxation and increase the momentum relaxation. The effective energy relaxation times at high fields are 24 and 65 ps for samples grown on sapphire and SiC substrates, respectively. They increase as the electron temperature decreases.

1 Introduction

Nitride compound semiconductors (III-V) are very attractive for high-power, high-frequency, and high-temperature electronics due to their larger bandgap, high breakdown field, and high spontaneous and piezoelectric polarization [1–5]. These advantages support the formation of high-power FETs and high electron mobility transistor (HEMT) structures with two-dimensional electron gas (2DEG) exceeding 10^{13} cm $^{-2}$ carrier density without doping [6]. When high-power FETs are subjected to an electric field that is applied in a plane of electron confinement, its operation critically depends on the hot-electron transport and the power dissipation controlled by the hot-electron temperature. The latter depends on the supplied electric power; this dependence can be treated in terms of the hot-electron energy relaxation time [7]. Knowledge of the relaxation time is a perquisite for FET engineering. Hot-electron effects are determined by electron-phonon interaction mechanisms and can provide valuable information about the nature of transport properties of elec-

tronic systems of modern semiconductors [8]. The hot-electron transport in nitrides has been studied using different electronic and optical based techniques: Microwave noise [9–13], Shubnikov-de Haas magnetoresistance [14–16], and Pump-probe Raman spectroscopy [17–19].

The dependence of the electron energy relaxation time on the electric field has revealed the transition from acoustic to polar optical phonon controlled electron energy dissipation [20, 21] and hot-phonon effects [22, 23]. From the hot-electron noise technique, the hot-phonon lifetime was reported to be ~ 0.5 ps for AlN/GaN 2DEG channels at 80 K [10] and ~ 0.36 ps for AlGaN/AlN/GaN at room temperature [11]. A comparable value of 0.29 ps was reported from the time-resolved pump-probe optical experiment for bulk GaN [24] at room temperature. For the GaN 2DEG channels, the phonon lifetime is 0.35 ± 0.1 ps at 373 K using microwave noise technique [25], 0.38 ps at room temperature with time-resolved experiments [26], and 0.45 ± 0.2 ps at 293 K [12] using microwave noise technique. The Raman pump-probe experiment on GaN has been reported to lead to a similar value of 0.35 ps at an electron density of 2×10^{19} cm $^{-3}$, which is comparable to that which is typical for the 2DEG channels [27].

^a e-mail: sibelgokden@gmail.com

The lifetime increases as the electron density decreases [27]. We should note that no systematic dependence of the lifetime on the hot-electron temperature has been found [12,28]. For the energy relaxation time the shortest relaxation time of 0.2 ps was reported using a femtosecond pump-probe technique [29]. At $n_s = 1.5 \times 10^{13} \text{ cm}^{-2}$, which is the two-dimensional electron density in GaN/AlGaN HEMT structures, relaxation time was found to be 0.7 ps at 77 K [30]. The dependence of phonon lifetime and energy relaxation times of AlGaN/GaN HEMT on substrate was solely studied [31]. Danilchenko et al. investigated energy dissipation comparatively in samples grown on sapphire and 4H-SiC substrates. In the case of sapphire substrate, the dissipation was described by the emission of optical phonons with an energy of 90 meV and a relaxation time of 25 fs. In the case of SiC substrate, it has been reported that both activation energy and relaxation time exceed the values characteristic of the electron-LO-phonon dissipation process. Buffer leakage currents and overheating of 2DEG were considered as the possible reasons responsible for the observed results.

Despite these successful results reported in the literature, hot-electron relaxation time studies pursue the understanding of the transport properties at the high field and the determination of the dominant scattering mechanisms for device performance in AlGaN/AlN/GaN 2DEG channel structures as both experimentally and theoretically. In the present work, a relatively simple method so-called mobility comparison technique together with the power balance conditions as described by Balkan et al. [30] is used to obtain the electron temperatures as a function of an applied electric field and the electron energy loss rate as a function of the electron temperature. We then compare our calculations for AlGaN/GaN HEMT structures grown by MOCVD on sapphire and SiC substrates and assess the differences arising due to varying substrate.

2 Experimental details and results

2.1 Hall measurements

AlGaN/AlN/GaN samples were grown using MOCVD on sapphire and 6H-SiC substrates. Both structures were grown at nearly similar conditions with almost the same structure and growth parameters. Before initiating the epitaxial growth, substrates were subjected to a heat process under a nitrogen environment at 1100 °C in order to clean oxides on the surface for 10 min. The growth process started with the growth of a ~15 nm thick low temperature (650 °C) AlN accumulation layer. A 0.5 μm thick AlN buffer layer was grown at 1150 °C. A ~2 μm thick undoped GaN template layer was grown at 1050 °C. To reduce the penetration of the electron wave function to the barrier layer and hence alloy scattering, an approximately 1.2 nm thick AlN spacer layer was grown at 1150 °C. Then, an AlGaN barrier layer of ~20 nm thick was grown over the spacer layer at 1050 °C. The growth process was finished with a ~3 nm thick GaN cap layer at 1050 °C.

Hall measurements were carried out using Van der Pauw geometry. Indium was annealed onto both samples to provide ohmic contacts. During the Hall measurements, current supply through the sample was deliberately kept low to ensure ohmic conditions; hence, the 2DEG was in thermal equilibrium with the lattice. The Hall measurements were performed at temperatures between 30 and 300 K using a variable temperature cryostat and electromagnet assembly for both samples.

Figure 1 shows the temperature-dependent Hall mobilities and electron density of the AlGaN/GaN heterostructures grown on sapphire and SiC. In case of the sample grown on sapphire, Hall mobility is $\mu = 12188 \text{ cm}^2/(\text{V s})$ and the two-dimensional electron density is $7.59 \times 10^{12} \text{ cm}^{-2}$ at $T = 30 \text{ K}$. While the Hall mobility decreases with temperatures up to $1699 \text{ cm}^2/(\text{V s})$ at 300 K electron density remains constant up to 130 K and then increases to $8.44 \times 10^{12} \text{ cm}^{-2}$ at 300 K. The increase in the carrier density at high temperatures is probably due to the temperature-induced thermal excitation of impurities in bulk GaN and AlGaN barrier layer. These temperature behaviors of 2DEG sheet densities imply that the conduction is dominated nearly exclusively by the carriers at the AlN/GaN heterointerfaces [32]. In case of the sample being grown on SiC substrate, the Hall mobility is measured $\mu = 11176 \text{ cm}^2/\text{V s}$ at 30 K. It decreases down to $\mu = 1830 \text{ cm}^2/\text{V s}$ at room temperature. The carrier density has no temperature dependence that is constant to an approximate value of $6 \times 10^{12} \text{ cm}^{-2}$. Sheet resistivities were obtained as $85 \Omega/\text{sq}$ and $112 \Omega/\text{sq}$ at 80 K for the samples grown on sapphire and 6H-SiC substrates, respectively. These values suggest that our samples had good crystalline quality. Since Hall data could not be produced above 300 K due to limitation of the experimental setup, possible mobility values were deduced by applying a theoretical fit which included main scattering processes, such as acoustic and optical phonon scattering, interface roughness, background impurity and alloy scatterings. These data were used to extract the electron temperature in mobility comparison method. As seen in the figure the excellent agreement of the theoretical and experimental mobility data below room temperature encourages us to use the expected mobility values at temperatures above 300 K.

2.2 *I-V* measurements

For pulsed *I-V* measurements, a simple bar geometry with length $L = 48 \mu\text{m}$ and width $w = 5 \mu\text{m}$ was used. Short bias pulses were applied to minimize Joule heating. In these measurements, voltage pulses of 400 ns duration were applied along the length of the sample up to a maximum electric field of $F = 25 \text{ kV cm}^{-1}$. Both the applied voltage and current through the sample were measured using a 500 MHz oscilloscope.

Figure 2 shows the electron drift velocity-electric field characteristics for AlGaN/GaN heterostructures grown on sapphire and 6H-SiC at 80 K. Electric field and drift velocity are calculated from the current-voltage characteristics.

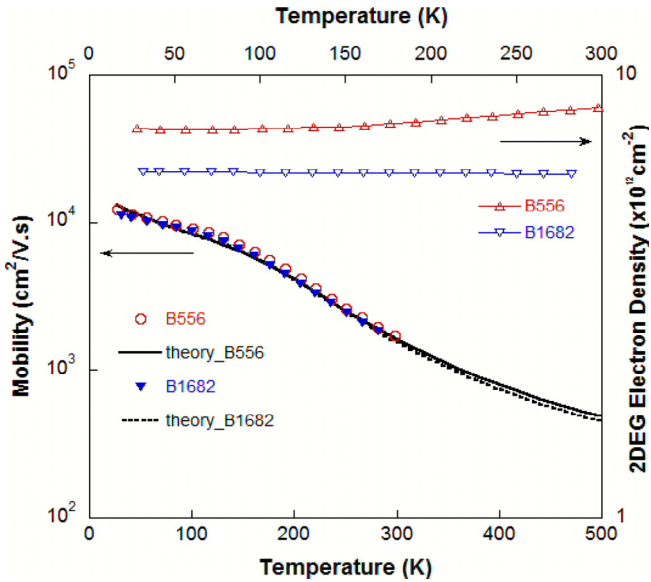


Fig. 1. (Color online) Two-dimensional electron density and Hall mobility versus temperature. Open circles show Hall mobility and open triangles show electron density for AlGaN/GaN heterostructures grown on sapphire. The filled reverse triangles show Hall mobility and the open reverse triangles show the two-dimensional electron density for AlGaN/GaN heterostructures grown on SiC. The line and dashed line are the calculated data using Matthiessen's rule theoretically for samples grown on sapphire and SiC substrates, respectively.

At low fields, the drift velocity exhibits linear behavior, but at higher fields (>3 kV) it deviates from linearity. When the effect of Joule heating is minimized through the application of nanosecond pulses of voltage, no velocity saturation is reached at fields up to 25 kV/cm. The estimated drift velocity is near 6.55×10^6 cm/s and 6.60×10^6 cm/s at approximately 25 kV/cm for the sample grown on sapphire and SiC substrates, respectively.

3 Mobility comparison method

In the present work, we investigated and compared the hot-electron dynamics of AlGaN/GaN HEMT structures grown by MOCVD on sapphire and SiC substrates using the mobility comparison method with power balance equations. This method was also successfully used for GaAs [33, 34], bulk GaN [35, 36], and two-dimensional AlGaN HEMT structures [30]. It involves the measurement of both the electric field dependence of the mobility (μ_E) at a fixed lattice temperature, and the lattice temperature dependence of the mobility at a fixed low electric field. The two sets of results are then normalized with respect to low-field mobility and low-temperature mobility, respectively. By comparing the two plots, it is possible to obtain the electron temperature as a function of the electric field.

Figure 3 shows the plots of the normalized mobility values versus lattice temperature and electric field for both samples. In Figure 4, the electron temperatures obtained

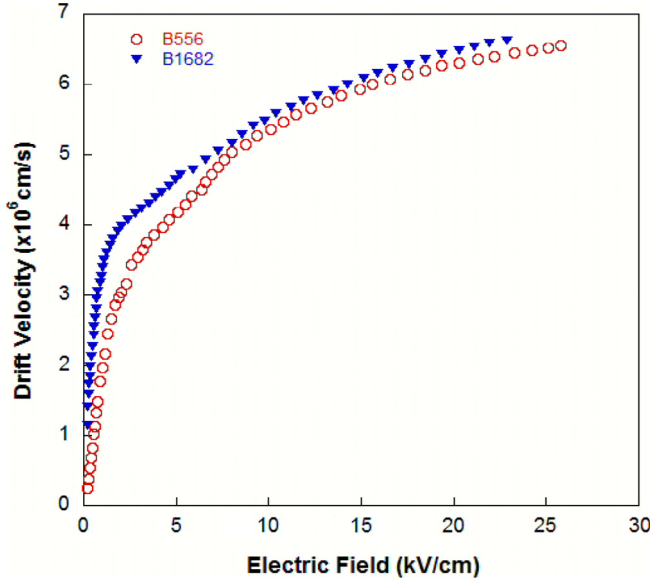


Fig. 2. (Color online) Drift velocity-electric field characteristics for the sample grown on sapphire (\circ) and SiC (\blacktriangledown) substrates at different ambient temperatures.

from the mobility comparison method by comparing the two plots for the AlGaN/GaN heterostructures grown on sapphire (B556) and SiC (B1682) substrates are shown. Because of the absence of Hall data above 300 K, Hall mobility versus the temperature data calculated with Matthiessen's rule was used to take into account the dominant scattering mechanisms theoretically. As seen in the figure the electron temperatures increase at two different rates. They increase gradually up to the electric field of 3 kV/cm and then monotonically above this field for both samples. Besides, the rate of increase in electron temperature for sample grown on SiC substrate is larger than that of sample grown on sapphire substrate. While the electron temperatures for both samples are close to each other at low electric field, they differ in larger extent at high fields.

It is noteworthy that the accuracy of the mobility comparison method assumes that

- (1) the carrier density does not change with the field;
- (2) the e - e scattering rate thermalizes the hot electrons among themselves, hence the non-equilibrium electron distribution can be represented by an electron temperature that is greater than the lattice temperature;
- (3) the dependence of the momentum relaxation on electron temperature (electric field) is identical to its dependence on the lattice temperature. The variation of the low-field mobility with the lattice temperature, in the LO-phonon regime, involves the emission and absorption of LO phonons randomly distributed in the k space with the electrons and phonons in thermal equilibrium with the lattice, i.e., $T_e = T_p = T_L$ (T_p is the 'phonon' temperature).

Therefore, the following conditions must hold:

- (i) at high fields, non-equilibrium phonons must exist;

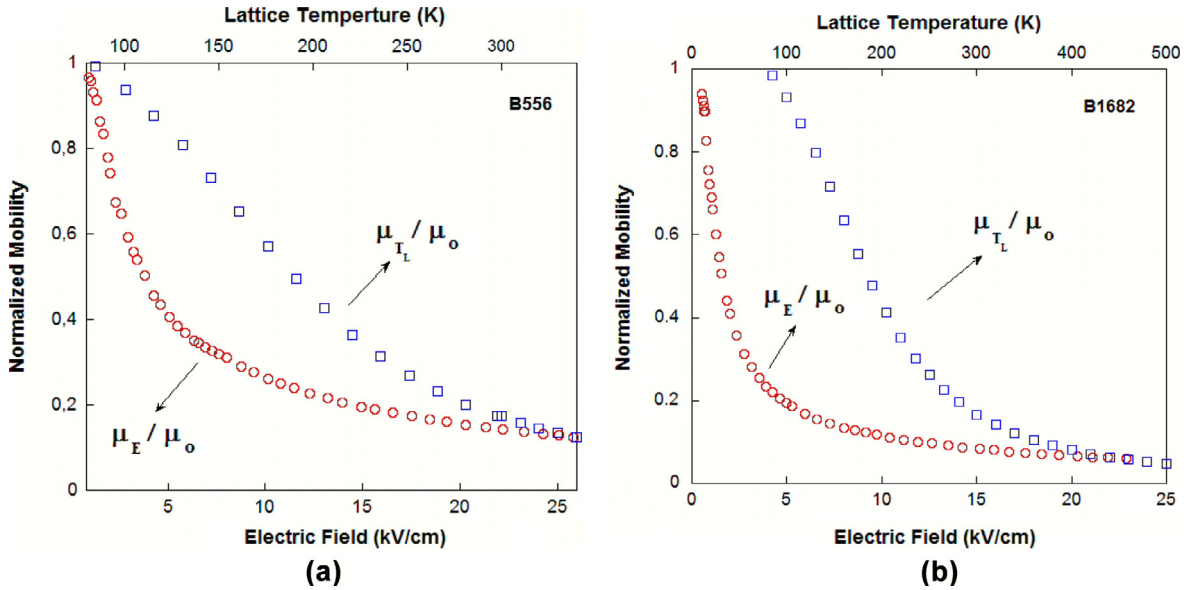


Fig. 3. (Color online) Field-dependent electron mobility at $T_L = 80$ K normalized with respect to the ohmic mobility, and the temperature-dependent mobility normalized with respect to the ohmic mobility for samples grown on (a) sapphire (B556) and (b) SiC (B1682) substrates, respectively.

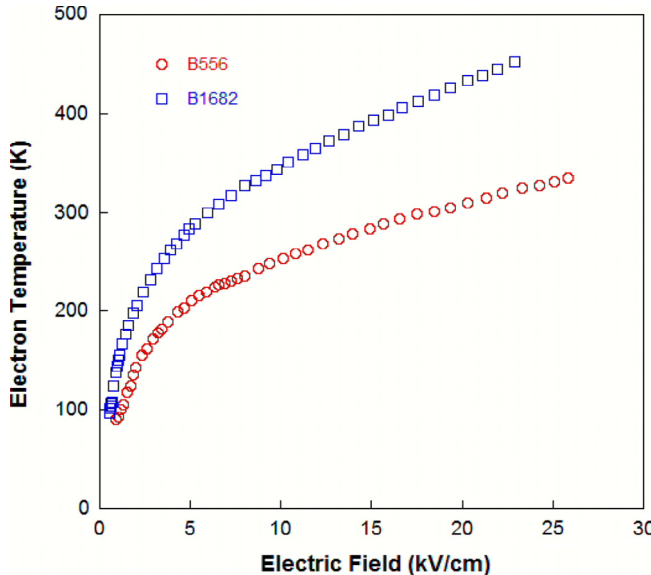


Fig. 4. (Color online) Electron temperature versus the electric field for the sample grown on sapphire (o) and SiC (square) substrates.

- (ii) the characteristic temperature of the hot phonons must be close to the electron temperature and
- (iii) the hot-phonon distribution at high fields should be randomized in k space, as it is at low fields.

If any of these conditions is not satisfied, the electron temperatures and hence the energy relaxation rates obtained from the mobility comparison experiment will be wrong.

In the steady state, the input power is equal to the power loss to the lattice through scattering processes. Therefore, electron energy loss mechanisms and rates

can be determined from the electron temperature dependence of the power loss using the power balance equations [37]:

$$p = e\mu E^2, \quad (1)$$

where μ is the mobility at electric field E . At high electric fields the electrons relax emitting LO phonons and thus reduce in energy and momentum. An expression for the power loss due to optical phonon emission and absorption can be written in the form:

$$p = \frac{\hbar\omega}{\tau_0} \left(\exp\left(-\frac{\hbar\omega}{kT_e}\right) - \exp\left(-\frac{\hbar\omega}{kT_L}\right) \right), \quad (2)$$

where τ_0 is the time constant for the e -LO interaction:

$$\tau_0 = \left[\frac{e^2\omega}{2\pi\hbar} \left(\frac{m^*}{2\hbar\omega} \right)^{1/2} \left(\frac{1}{\varepsilon_\infty} - \frac{1}{\varepsilon_s} \right) \right]^{-1}, \quad (3)$$

where $\varepsilon_\infty, \varepsilon_s$ are the high frequency and static permittivities, and $\hbar\omega$ is the LO-phonon energy. Taking for GaN $m^* = 0.22m_0$, $\varepsilon_\infty = 5.35\varepsilon_0$, $\varepsilon_s = 9.7\varepsilon_0$ and the e -LO-phonon energy $\hbar\omega = 92$ meV, we find the scattering time $\tau_0 = 8$ fs. The e -LO phonon scattering time constant τ_0 is replaced by the effective energy relaxation time, τ_{eff} , which takes into account all the hot-phonon effects:

$$p = \frac{\hbar\omega}{\tau_{\text{eff}}} \left(\exp\left(-\frac{\hbar\omega}{kT_e}\right) - \exp\left(-\frac{\hbar\omega}{kT_L}\right) \right). \quad (4)$$

In the high-temperature regime, an expression for the power loss due to acoustic phonon emission can be expressed [35]:

$$p = (C_{np} + C_p)(kT_e - kT_L), \quad (5)$$

where

$$C_{np} = \frac{3\Xi^2 m^{*2}}{2\rho\hbar^3 L_z} \quad (6)$$

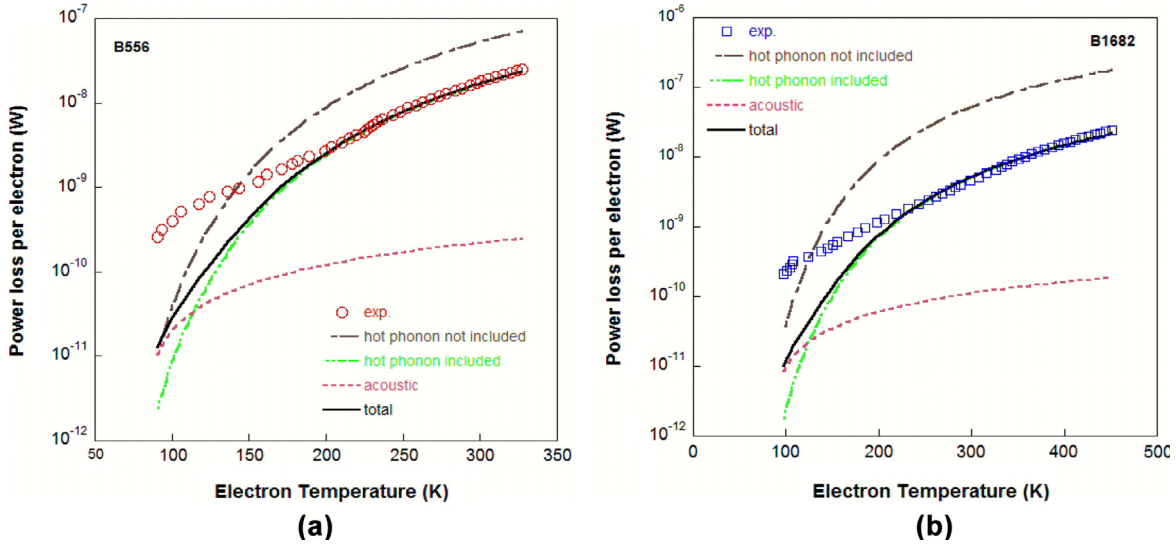


Fig. 5. (Color online) Power loss per electron versus an electron temperature at 80 K lattice temperature for the samples grown on (a) sapphire substrate and (b) SiC substrate. Circles: Experimental power loss per electron. Gray: Theoretical power loss obtained from equation (2). Green: Theoretical power loss obtained from equation (4). Pink: Theoretical power loss via acoustic phonon emission. Line: Theoretical power loss per electron via acoustic phonons and optical phonons.

and

$$C_p = \frac{3e^2 K_{av}^2 m^* V_s^2}{4\pi\epsilon\hbar^3 L_z N_{2D}} \quad (7)$$

are the magnitudes of the deformation potential and piezoelectric interactions, respectively. Here, Ξ is the acoustic deformation potential, ρ is the density, L_z quantum is the well width, V_s is the speed of sound in the material, and K_{av} is the average electromechanical coupling constant. Taking for GaN $\Xi = 8.3$ eV, $\rho = 6.15 \times 10^{-3}$ kg/m³, $L_z = 65$ Å, $V_s = 2.16 \times 10^3$ m/s, $K_{av}^2 = 0.039$.

Power loss per electron versus the electron temperature of the AlGaN/GaN heterostructures grown on sapphire and SiC substrates is plotted in Figure 5. The acoustic phonon emission seemed to be ineffective in the energy relaxation processes over all fields. Theoretical power loss which does not include the hot-phonon effects (Eq. (2)) does not fit our experimental data. Due to disagreement between our experimental results we used equation (4) which takes into account the non-drifting hot-phonon effects. This indicates that the optical phonon scattering arising hot-phonon production is the dominant energy loss mechanism at high electron temperatures. The solid line represents theoretical power loss per electron via acoustic phonons and optical phonons which include hot-phonon effects. Excellent agreement is satisfied specially at high fields. As seen in the figure, the experimental loss rates are significantly higher than the theoretically expected ones at low electron temperatures. There is an order of magnitude difference between theory and experiment at the electron temperature of 100 K. The reason for the observed disagreement between the experimental and the theoretical loss rates at low electron temperatures might be the failure of one of the other assumptions made in the mobility comparison method, or due to ineffectiveness of the hot-phonon effect.

4 Conclusions

We studied the hot-electron dynamics of AlGaN/GaN HEMT structures grown by MOCVD on sapphire and SiC substrates comparatively by the mobility comparison method with power balance equations. Drift velocities obtained from pulsed current-voltage measurements are 6.55×10^6 cm/s and 6.6×10^6 cm/s at an electric field of around $E \sim 2.5$ kV/cm at 80 K, for AlGaN/GaN heterostructures grown epitaxially on sapphire and SiC, respectively. Using the mobility comparison method, electron temperatures are obtained as a function of the applied electric field and power loss rates are obtained as a function of electron temperature. Electron temperatures for SiC substrate are higher than those for sapphire substrate. This difference might arise due to the lower thermal resistance of SiC in comparison to Al₂O₃. The power loss results are compared with the theoretical calculations based on the assumption of hot-phonon production at high fields. We have seen an agreement between the experimental results and the theoretical calculations toward high electron temperatures. At low electron temperatures, our experimental values deviate from the theoretical value. In this regime other scattering mechanisms might be responsible for this discrepancy. The mobility comparison method works for AlGaN HEMT structures at high electron temperatures. However, at low electron temperatures this method is not suitable for investigating hot-electron transport. The reason for the observed disagreement between the experimental and theoretical loss rates might be the failure of one of the other assumptions made in the mobility comparison method. We also found that the LO-phonon lifetime is 500 fs and 320 fs for sapphire and SiC substrates, respectively. The long hot-phonon lifetime results in large non-equilibrium hot phonons. Non-equilibrium hot phonons slow energy

relaxation and increase the momentum relaxation. The effective energy relaxation times at high fields are 24 and 65 ps for samples grown on sapphire and SiC substrates, respectively. They increase as the electron temperature decreases.

References

1. O. Ambacher et al., J. Appl. Phys. **85**, 3222 (1999)
2. S.J. Pearton, J.C. Zolper, R.J. Shul, F. Ren, J. Appl. Phys. **86**, 1 (1999)
3. S. Nakamura, G. Fasol, *The Blue Laser Diode* (Springer Verlag, Berlin, 1997)
4. S.T. Sheppard, K. Doverspike, W.L. Pribble, S.T. Allen, J.W. Palmour, L.T. Kehias, T.J. Jenkins, IEEE Trans. Electron. Devices Lett. **20**, 161 (1999)
5. S. Strite, H. Morkoc, J. Vac. Sci. Technol. B **10**, 1237 (1992)
6. J. Kuzmik, IEEE Trans. Electron. Devices Lett. **22**, 510 (2001)
7. A. Matulionis, J. Liberis, E. Šermukšnis, J. Xie, J.H. Leach, M. Wu, H. Morkoc, Semicond. Sci. Technol. **23**, 075048 (2008)
8. M. Ari, O. Turkoglu, Physica B **348**, 272 (2004)
9. A. Matulionis, R. Katilius, J. Liberis, L. Ardaravicius, L.F. Eastman, J.R. Shealy, J. Smart, J. Appl. Phys. **92**, 4490 (2002)
10. A. Matulionis, J. Liberis, L. Ardaravicius, J. Smart, D. Pavlidis, S. Hubbard, L.F. Eastman, Int. J. High Speed Electron. Syst. **12**, 459 (2002)
11. A. Matulionis, J. Liberis, M. Ramonas, I. Matulioniene, L.F. Eastman, A. Vertiatchikh, X. Chen, Y.-J. Sun, Phys. Stat. Sol. (c) **2**, 2585 (2005)
12. A. Matulionis, Phys. Stat. Sol. (a) **203**, 2313 (2006)
13. A. Matulionis, J. Liberis, L. Ardaravicius, M. Ramonas, I. Matulioniene, J. Smart, Semicond. Sci. Technol. **17**, L9 (2002)
14. K.J. Lee, J.J. Harris, A.J. Kent, T. Wang, S. Sakai, D.K. Maude, J.-C. Portal, Appl. Phys. Lett. **78**, 2893 (2001)
15. A.F. Brana, C. Diaz-Paniagua, F. Batallan, J.A. Garrido, E. Munoz, F. Omnes, J. Appl. Phys. **88**, 932 (2000)
16. C.E. Martinez, N.M. Stanton, A.J. Kent, M.L. Williams, I. Harrison, H. Tang, J.B. Webb, J.A. Bardwell, Semicond. Sci. Technol. **19**, S440 (2004)
17. D. Von der Linde, J. Kuhl, H. Klingenburg, Phys. Rev. Lett. **44**, 1505 (1980)
18. J.A. Kash, J.C. Tsang, J.M. Hvam, Phys. Rev. Lett. **54**, 2151 (1985)
19. S.S. Jha, A.S. Vengurlekar, Hyperfine Interact. **38**, 585 (1987)
20. K.T. Tsen, D.K. Ferry, A. Botchkarev, B. Sverdlov, A. Salvador, H. Morkoc, Appl. Phys. Lett. **72**, 2132 (1998)
21. G.P. Srivastava, Phys. Rev. B **77**, 155205 (2008)
22. M. Ramonas, A. Matulionis, J. Liberis, L. Eastman, X. Chen, Y.-J. Sun, Phys. Rev. B **71**, 075324 (2005)
23. B.K. Ridley, Semicond. Sci. Technol. **4**, 1142 (1989)
24. S. Wu, P. Geiser, J. Jun, J. Karpinski, D. Wang, R. Sobolewski, J. Appl. Phys. **101**, 043701 (2007)
25. A. Matulionis, J. Liberis, I. Matulioniene, M. Ramonas, L.F. Eastman, J.R. Shealy, V. Tilak, A. Vertiatchikh, Phys. Rev. B **68**, 035338 (2003)
26. Z. Wang, K. Reimann, M. Woerner, T. Elsaesser, D. Hofstetter, J. Hwang, W.J. Schaff, L.F. Eastman, Phys. Rev. Lett. **94**, 037403 (2005)
27. K.T. Tsen, J.G. Kiang, D.K. Ferry, H. Morkoc, Appl. Phys. Lett. **89**, 112111 (2006)
28. A. Matulionis, J. Liberis, L. Ardaravicius, L.F. Eastman, J.R. Shealy, A. Vertiatchikh, Semicond. Sci. Technol. **19**, S421 (2004)
29. H. Ye, G.W. Wicks, P.M. Fauchet, Appl. Phys. Lett. **74**, 711 (1999)
30. N. Balkan, M.C. Arikan, S. Gokden, V. Tilak, B. Schaff, R.J. Shealy, J. Phys. Condens. Matter **14**, 3457 (2002)
31. B.A. Danilchenko, S.E. Zelensky, E. Drok, S.A. Vitusevich, S.V. Danylyuk, N. Klein, H. Lüth, A.E. Belyaev, V.A. Kochelap, Phys. Stat. Sol. (b) **243**, 1529 (2006)
32. R. Tülek, A. Ilgaz, S. Gökden, A. Teke, M.K. Özturk, M. Kasap, S. Ozcelik, E. Arslan, E. Özbay, J. Appl. Phys. **105**, 013707 (2009)
33. N. Balkan, R. Gupta, M.E. Daniels, B.K. Ridley, M. Emeny, Semicond. Sci. Technol. **5**, 986 (1990)
34. R. Gupta, N. Balkan, B.K. Ridley, Semicond. Sci. Technol. **7**, 274 (1992)
35. N.M. Stanton, A.J. Kent, A.V. Akimov, P. Hawker, T.S. Cheng, C.T. Foxon, J. Appl. Phys. **89**, 973 (2001)
36. N.M. Stanton, A.J. Kent, A.V. Akimov, P. Hawker, T.S. Cheng, C.T. Foxon, Phys. Stat. Sol. (a) **176**, 369 (1999)
37. M. Cankurtaran, H. Çelik, N. Balkan, Phys. Stat. Sol. (b) **229**, 1191 (2002)